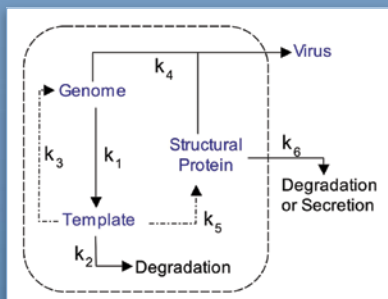


## Spectral methods for sensitivity analysis of stochastic dynamical systems

Given recent advances in nanotechnology, many phenomena can now be studied quantitatively on a molecular level. At this scale, stochastic, or random, effects often play a significant role in system behavior. Particularly in the biological context, random noise can be crucial in the dynamical behavior of gene regulatory networks in cells, affecting, for example, the switching of the system state between different basins of attraction. To aid in the analysis of such systems, we are developing tools based on the use of spectral expansions to represent random variables. These methods build on previous work done at the Combustion Research Facility in the area of uncertainty quantification in reacting flows and microfluidics.



**Figure 1.** Intracellular viral kinetics model for a non-lytic virus, developed by Srivastava et al. (2002). Dash-dot lines represent catalytic reactions.

As an example of a simple gene regulatory network, Figure 1 shows a simplified biochemical model of the intracellular kinetics that govern gene regulation when a cell is infected by a non-lytic virus. Contrary to lytic viruses, a non-lytic virus avoids overcrowding its host cell with viral progeny so as to not burst it open. Therefore a non-lytic

(Continued on page 5)

## Soot formation under heavy-EGR conditions

Modern diesel engines use exhaust-gas recirculation (EGR) to control nitrogen-oxide ( $\text{NO}_x$ ) emissions. While EGR reduces combustion flame temperatures, leading to reduced  $\text{NO}_x$  emissions, reducing charge-gas oxygen levels and lowering combustion temperature can also mean that the soot formed is incompletely oxidized, causing increased particulate matter (PM) emissions. Thus, the use of EGR commonly results in a classic PM- $\text{NO}_x$  tradeoff that prevents low-emission combustion.

CRF researchers Lyle Pickett and Cherian Idicheria are working to address the challenge of high-EGR soot formation and to develop methods for mitigating engine-out PM.

It is difficult to fully understand how soot forms at high-EGR conditions because there are many competing factors when using EGR in engines. EGR reduces the intake oxygen mole fraction; EGR use often causes an increase in the intake temperature as well. EGR cooling is employed in engines to minimize this temperature increase, but the heavy EGR flow rates required for  $\text{NO}_x$  control (often greater than 50%), particularly at high engine load, can cause significant temperature increases. As a consequence, the charge-gas temperature at the time of combustion is higher than conditions without EGR. Another consequence of heavy-EGR use is that intake pressure

is increased (through turbocharging or supercharging) to deliver needed oxygen in-cylinder as a means of compensating for the oxygen that was displaced by EGR. This causes elevated gas pressures and densities at the time of combustion.

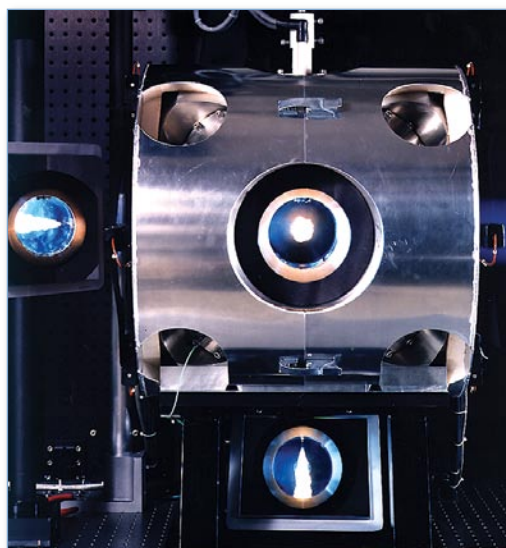


**Figure 1.** Constant-volume combustion chamber with reacting diesel spray.

Pickett and Idicheria performed soot measurements in reacting diesel sprays while varying ambient temperature, density, and oxygen concentration to provide a fundamental understanding of how these variables affect soot formation. They used laser-induced incandescence and laser-extinction while varying conditions in a constant-volume combustion chamber (Figure 1) to generate a dataset of the local soot volume fraction ( $f_v$ ) within the spray (Figure 2). The dataset is the

(Continued on page 2)

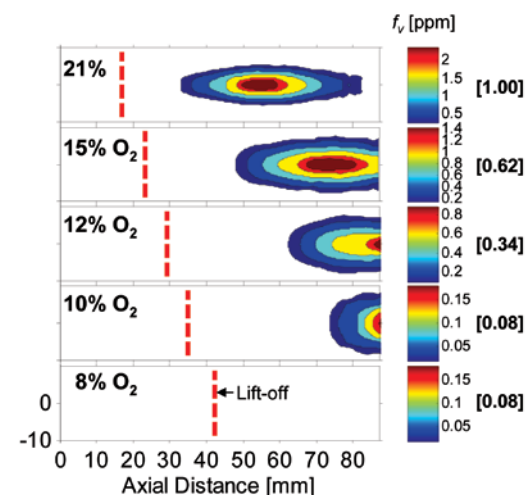


**Figure 2.** Soot volume fraction distributions as function of ambient oxygen concentration. Ambient conditions: 1000 K, 14.8 kg/m<sup>3</sup>. Injector conditions: 1500 bar, 0.1 mm nozzle diameter, fuel=n-heptane. Dashed line is lift-off length.

## Soot formation (Continued from page 1)

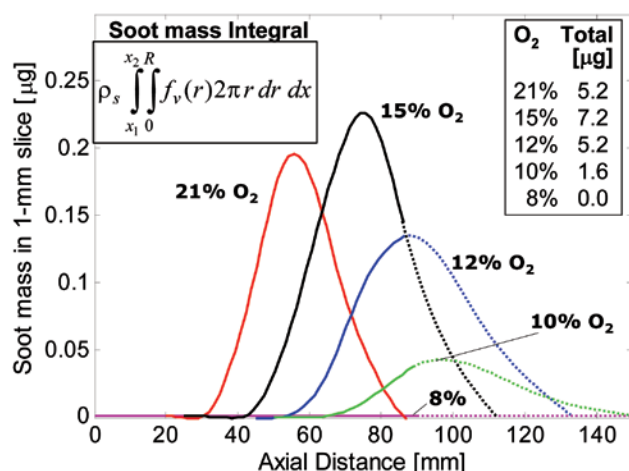


**Figure 3.** Soot mass in thin (1 mm) radial cross-sections of the jet as a function of axial distance.

first of its kind for diesel sprays.

Figure 2 shows that a decrease in ambient oxygen concentration (simulating an increase in EGR) at a typical engine charge-gas temperature, causes a decrease in the local soot volume fraction. Brackets at the right indicate the relative decrease in the colorbar scale. Using EGR also causes the soot position to shift farther downstream in the jet. This shift is partly caused by the lack of ambient oxygen, as sprays must mix with more ambient gas to complete combustion. An important implication of this result is that soot formation processes have longer residence time for high-EGR conditions.

Although  $f_v$  decreases, the total mass of soot in the jet actually increases, reaches a peak at 15% O<sub>2</sub> and then decreases to zero at 8% O<sub>2</sub> (Figure 3). This trend in soot formation is caused by competition between soot formation rates and increasing residence time. Soot formation rates decrease with decreasing oxygen concentration because of the lower combustion temperatures. Simultaneously, the residence time for soot formation increases, allowing more time for accumulation of soot. The tradeoff between an increased residence time and a reduced rate of soot formation determines the ambi-

ent oxygen concentration for which soot formation is maximized. For these typical engine temperatures and densities, this maximum is 15% O<sub>2</sub>.

An increase in ambient temperature, which is likely when using EGR, significantly changes the oxygen level of maximum soot production. Figure 4 shows the maximum soot mass in an axial soot

distribution (i.e. Figure 3) as a function of ambient temperature. Elevated ambient temperatures (>1000 K), in combination with high EGR, cause a major increase in soot formation. Soot increases with increasing ambient temperature for all levels of EGR, but the increase in soot is much more substantial for an high-EGR ambient (10% O<sub>2</sub>) compared to an ambient with no EGR (21% O<sub>2</sub>). High-EGR, high-ambient-temperature conditions lead to higher soot levels because residence time and soot formation rates are both high. Low-ambient-temperature (<1000 K), high-EGR

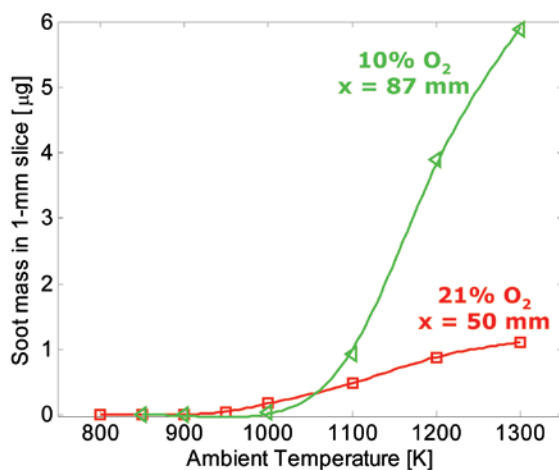


**Figure 4.** Soot mass in thin (1 mm) cross-section of the jet, corresponding to axial position of peak soot, plotted as a function of ambient temperature for two different ambient oxygen concentrations.  $\rho_a = 14.8 \text{ kg/m}^3$ .


conditions create much less soot production because soot formation rates are low and dominate over the increased residence time. These results emphasize the importance of EGR-cooling and temperature control to keep soot levels low.

An increase in ambient gas density and pressure at the time of combustion also causes a significant increase in soot formation (Figure 5). In addition, soot forms much closer to the nozzle. Some increase in soot is expected because of the higher ambient density, which tends to compress the soot formation and

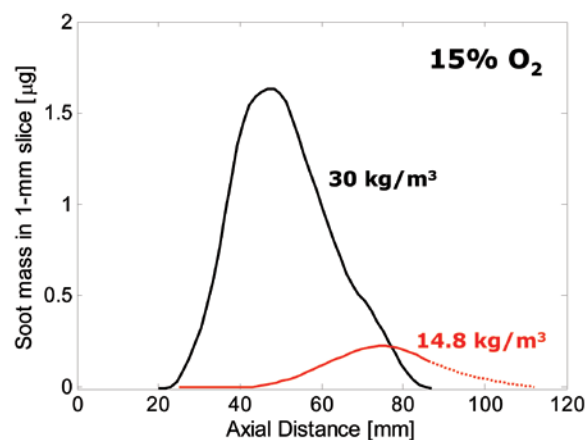


**Figure 5.** Comparison of soot mass distributions at two ambient densities.  $T_a = 1000 \text{ K}$ .

oxidation processes into a shorter axial distance. Nevertheless, the total soot integrated along the jet axis is substantially higher at 30 kg/m<sup>3</sup> compared to 14.8 kg/m<sup>3</sup>.

This investigation provides new information about soot formation for modern low-temperature combustion engines. Understanding the processes affecting in-cylinder soot formation is critical in order to ultimately reduce engine-out PM. The quantitative datasets of in-situ soot volume fraction can be used for the development and validation of computational models. Accordingly, the soot data at these conditions, and other supporting data, is available to download at the newly-opened Engine Combustion Network website (<http://www.ca.sandia.gov/ecnl/>). 



## TNF WORKSHOP

HEIDELBERG, GERMANY • AUGUST 3-5, 2006

### The Eighth International Workshop on Measurement and Computation of Turbulent Nonpremixed Flames (TNF8)

held August 3-5 in Heidelberg, Germany, was attended by 80 participants from 14 countries. TNF8 marks a decade of collaboration among experimental and computational researchers seeking to better understand turbulent combustion at a fundamental scientific level and to validate advanced computational combustion models. The workshop has focused on interactions of turbulence and chemistry in relatively simple flames, which allow for comprehensive measurements and unambiguous comparisons with model predictions. By providing a framework for comparing multiple modeling approaches against detailed data from a progression of turbulent flames, the TNF series has helped to catalyze progress



in modeling of turbulent nonpremixed and partially premixed combustion. According to Rob Barlow, the primary organizer of the workshop, its success has stemmed from the willingness of a core group of people to invest significant time and effort beyond their individual research activities. Current members of the TNF Organizing Committee include Bob Bilger (Sydney University), J.-Y. Chen (UC Berkeley), Andreas Dreizler (Technical University of Darmstadt), Johannes Janicka (Technical University of Darmstadt), Peter Lindstedt (Imperial College), Assaad Masri (Sydney University), Joe Oefelein (Sandia), Heinz Pitsch (Stanford), Steve Pope (Cornell), Dirk Roekaerts (Delft University), and Luc Vervisch (INSA de Rouen).

Key discussion topics (and session coordinators) for TNF8 included comparisons of measured and modeled results for bluff-body and swirl-stabilized flames (Andreas Kempf, Imperial College), modeling



strategies for chemistry and mixing (J.-Y. Chen, UC Berkeley), progress on measurements of scalar dissipation (Rob Barlow, Sandia and Noel Clemens, UT Austin), new experimental capabilities based on high-speed diagnostics (Andreas Dreizler, TU Darmstadt), quality assessment for large eddy simulation (Markus Klein, TU Darmstadt and Joe Oefelein, Sandia), issues for comparing LES and experiments (Andreas Kronenbourg, Imperial College and Venkat Raman, UT Austin), potential contributions from DNS (Evatt Hawkes, Sandia), and challenges for validation of premixed combustion models (Johannes Janicka, TU Darmstadt). There was also lively discussion of priorities and possible directions for future TNF Workshop collaborations. The complete proceedings will be available before the end of the year at <http://www.ca.sandia.gov/TNF>



### Jackie Chen joins board of Combustion Institute



CRF researcher Jackie Chen was nominated for a six year term on the board of directors of the Combustion Institute along with Meredith M. Colket, United Technologies Corp; R. Peter Lindstedt, Imperial College, USA; Reginald R. Mitchell, Stanford University; Derek Dunn-Rankin, University of California- Irvine; and Mitchell B. Smooke, Yale University. Don Hardesty retired from the board.

### Visiting researcher from Norway's Sintef

Stig Rune Sellavag is visiting the CRF for six months from Sintef Energy Research, in Trondheim, Norway. Sintef is a private umbrella group for several research institutes, including two groups working on gas technology and combustion, as well as a group working on combustion of organic waste such as municipal trash.

At the CRF, Sellavag focuses on combustion kinetics, working with Yuri Georgievski, Jim Miller, and Stephen Klippenstein. Their research is connected to modeling combustion of hydrogen in gas turbine conditions and calculating the rates of certain elementary reactions involved in the combustion of hydrogen.

### Claudiu Gradinaru joins University of Toronto



Claudiu Gradinaru, a post doc with Carl Hayden, has taken up a position at the Department of Chemical and Physical Sciences at the University of Toronto at Mississauga. While at the CRF, Gradinaru conducted time-resolved single molecule fluorescence microscopy to study protein and DNA dynamics.



**Ramanan Sankaran**

Ramanan Sankaran, a postdoc working with Jackie Chen on terascale direct numerical simulations (DNS) of turbulent combustion, will be joining the Leadership Computing Facility at Oak Ridge National Laboratory in September, 2006.

At the CRF, Sankaran was involved in porting and optimizing the Sandia DNS code, S3D, to the Cray X1E and CrayXT3 machines at Leadership Class Computing Facility (LCF) at Oak Ridge National Laboratories (ORNL) where he subsequently performed terascale DNS of lean premixed methane/air turbulent Bunsen flames.

## Characterization of hydrogen flames for safety codes and standards development

One barrier to the development of a hydrogen economy and its associated technologies is the lack of tested safety codes and standards. Such codes and standards are necessary to assure that related products and systems are safe and perform as designed. Indeed, a well-developed set of codes and standards governs most components related to our current hydrocarbon-based energy infrastructure. Thus, the development of an infrastructure for the future hydrogen economy will require the simultaneous development of an analogous set of safety codes and standards.

A Sandia team consisting of Robert Schefer, Alejandro Molina (former postdoc), Tim Williams (postdoc), and Bill Houf are developing the technical basis for assessing the safety of hydrogen-based systems and for the definition of relevant codes and standards. The project impacts most areas of

hydrogen ignition, combustion, and subsequent heat transfer from hydrogen flames. Technical information is contained in simple engineering models that are used for rapid assessment of different scenarios and risk analyses.

One scenario of particular interest is a hydrogen jet issuing from a high-pressure source into surrounding air. This is analogous to an unintended release scenario that might result from a high-pressure leak in a hydrogen delivery system. A relevant safety question is, what would be the radiative heat transfer rates from a flame formed if the hydrogen jet is accidentally ignited? To determine the answer, the hydrogen-jet flame shown in Figure 1 has been studied extensively. Tests of the largest flames were carried out in collaboration with SRI



Photograph of hydrogen jet flame.

International at their Corral Hollow test site in Tracy, CA.

hydrogen utilization, including bulk transportation and distribution, storage, production and utilization. The team is developing benchmark experiments and a defensible analysis strategy for risk and consequence assessment of unintended releases from hydrogen systems. This work includes

experimentation and modeling to understand the fluid mechanics and dispersion of hydrogen for different release scenarios, including investigations

In the tests, the hydrogen is supplied through a 5-mm diameter fuel tube located at the bottom of the photograph and oriented in the vertical direction. The hydrogen is supplied by storage tubes at pressures up to 413 bar. At these conditions, the flame is about 9 meters in length; smaller flames are produced using lower pressures and smaller jet diameters. Visible and infrared video were obtained to evaluate flame length, diameter and structure, while radiometers placed along the length of the flame were used to determine the radiant heat flux. Similar measurements were carried out in smaller laboratory-scale flames in the Sandia CRF to better understand the effects of flame scaling.

Previous measurements in the literature have shown that the radiative heat flux from hydrocarbon-jet flames scales with the flame residence time,  $\tau_g$ . Shown in Figure 2 is the variation in

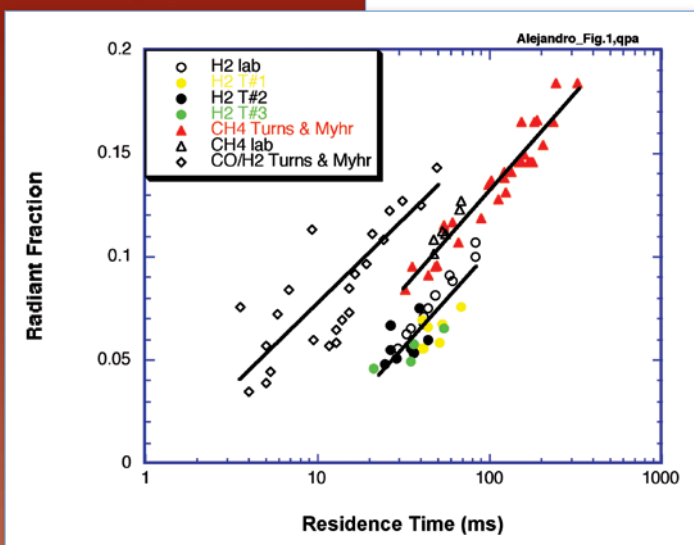


**Figure 1.** Variation of radiative fraction with global residence time for different fuels in jet flames.

(Continued on page 6)



## Spectral methods (Continued from page 1)

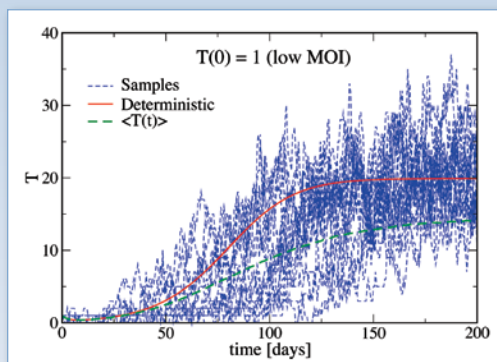


**Figure 2.** Sampling of simulated stochastic trajectories of the template (T) population for the network in Figure 1, for a low Multiplicity of Infection (MOI).

Simulated trajectories over time that show the behavior of the T population in this biochemical reaction network are shown in Figure 2 for the case where an infection consists initially of only one template molecule. Individual realizations (blue lines) of the T population exhibit significant variability. Some infections take off rapidly, while others are delayed or die off. Note also that the solution of the corresponding deterministic set of equations (red curve), where stochastic noise is neglected, is significantly different from the average of the individual stochastic realizations (green curve), even at late time. The main reason for this difference is that the stochastic model accounts for the possibility of failed infections whereas the deterministic model does not.

As shown in Figure 3, there is a significant probability of failure for infections that start out with just one T molecule. This is opposed to the deterministic model, which predicts that all infections go to the same steady state, and which therefore fails to account for a relevant aspect of the system behavior. Since stochastic effects are an integral part of the function of these systems, it is necessary to have proper tools to analyze their behavior. In this context, we have been developing spectral methods to enable sensitivity analysis of stochastic dynamical systems.

Sensitivity analysis is concerned with the assessment of the relative contribution of each of the parameters of a model on the observables of interest. Conventional sensitivity analysis

involves the evaluation of derivatives of the system output state with respect to the parameters of interest. In the present stochastic context, however, these derivatives are mathematically ill-defined, which necessitates alternate, effective sensitivity analysis strategies.

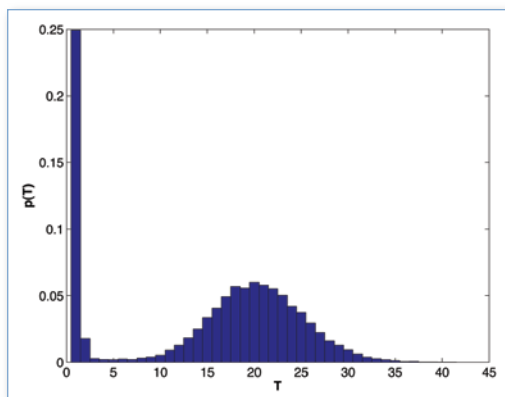


**Figure 3.** Probability density function of the number of T molecules 200 days after infection. The peak at  $T=0$  corresponds to the probability of failed infections.


In our work, sensitivity analysis is performed by, first,

virus needs to have a controlled replication mechanism. The network shown in Figure 1 has six reactions between three viral components: Template (T), Genome (G) and Structural Protein (S). An infection starts with one or more copies of T, which are used to generate copies of G and S. These components then combine to form viral progeny that is secreted from the cell.

assigning properly chosen perturbations to the parameters of interest. These parameters are modeled as random variables with specified distributions, defined by the chosen perturbations, and are represented with spectral polynomial chaos expansions. The random perturbations are then propagated through the dynamical system using sampling-based, non-intrusive spectral projection methods to obtain their effect on the observables of interest. The result is a response surface describing the dependence of the system response statistics on the parameters of interest, from which specific sensitivities are derived.

Figure 4 shows the sensitivity of the failed infection probability with respect to each of the rate constants in the above viral kinetics model. It is clear that the 2<sup>nd</sup> and 3<sup>rd</sup> rate constants have the dominant effect, which points at the relevance of the template decay and genome production reactions. The decay rate of S is also important, but only in the first days after infection. For more details on this analysis, please see the forthcoming paper in the Biophysical Journal by D. Kim, B. Debusschere and H. Najm.

This work will be expanded to include predictability analysis, while also improving the generality and robustness of these methods, to make them more widely applicable on larger-scale systems with both parametric and inherent uncertainties.

The application of the above analysis methods to stochastic dynamical systems enables more detailed study of their dynamics. This capability allows a more fundamental understanding of these systems, providing insight into dominant reactions that drive their observed dynamics; and can facilitate design of strategies to more effectively manipulate them. When applied to biosystems, for example, this analysis could help determine the gene regulation pathways most responsible for controlling the transition of a cell from a healthy to a diseased state, and which reactions would need to be targeted with drugs to bring the organism back to health. This work is funded by the DOE office of Mathematical, Information and Computational Sciences. 

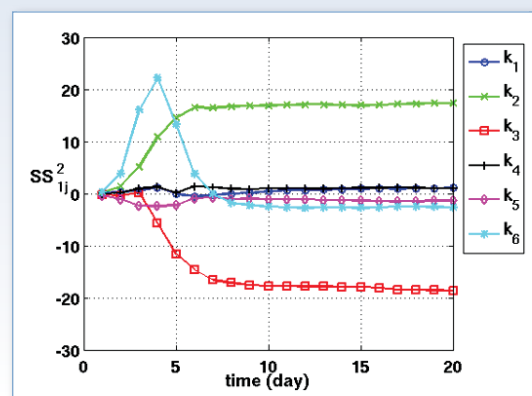


**Figure 4.** Sensitivity of the probability of infection failure with respect to the 6 model parameters as a function of the number of days after infection. The sensitivity coefficients quantify the change in the expected percentage of failures per fractional change in the model parameters.

RECRUITING, STAFFING & UNIVERSITY PARTNERSHIPS

JOBS

- Computational reacting flow research
- Reacting flow computations and analysis development
- Simulation and spectral analysis of stochastic dynamical systems
- Theoretical chemistry

<http://www.sandia.gov/employment/index.html>

# Characterization of hydrogen flames

(Continued from page 4)

the radiative fraction with flame residence time for non-sooting CO/H<sub>2</sub> and C<sub>3</sub>H<sub>8</sub> (propane) jet flames. The radiative fraction, X<sub>rad</sub>, is the fraction of combustion heat release that is emitted as thermal radiation. Also shown are results for the hydrogen flames. It can be seen for a given flame residence time, the CO/H<sub>2</sub> flames have the highest radiative fractions, followed by the CH<sub>4</sub> flames and that the radiative fraction from the hydrogen flames is about a factor of two lower than the CO/H<sub>2</sub> flames. Previously developed correlations for hydrocarbon flames suggest that radiative fraction scales solely with flame residence time and assumes constant radiative characteristics that do not depend on fuel composition. This approach does not consider variations in radiative characteristics, as combustion product gas composition and temperatures change due to variations in fuel composition. Dimensional analysis further yields the result that the radiative fraction is proportional to the product, a<sub>p</sub>T<sub>f</sub><sup>4</sup>τ<sub>g</sub>, where

a<sub>p</sub> is the Planck-mean absorption coefficient and T<sub>f</sub> is the flame temperature. In this formulation, a<sub>p</sub> is calculated from the known or estimated product gas composition and accounts for the different radiative properties of product gas species (primarily H<sub>2</sub>O and CO<sub>2</sub>), and T<sub>f</sub> is the flame temperature for the different fuels. Figure 3 shows the same values of X<sub>rad</sub> as Figure 2, but when plotted against the factor τ<sub>g</sub>a<sub>p</sub>T<sub>f</sub><sup>4</sup>, it can be seen that the data for CH<sub>4</sub>, CO/H<sub>2</sub> and H<sub>2</sub> flames collapse onto the same curve.

The factor that shows the most significant effect in normalizing the data for the different flames is a<sub>p</sub> and not T<sub>f</sub>. Further calculation shows that the difference in a<sub>p</sub> for the different fuels occurs because of the presence of thermal radiation bands for CO<sub>2</sub> in the CH<sub>4</sub> and CO/H<sub>2</sub> that are absent in the hydrogen flames. These bands are strongest for the CO/H<sub>2</sub> flames because of higher CO<sub>2</sub> concentration in the product gases.

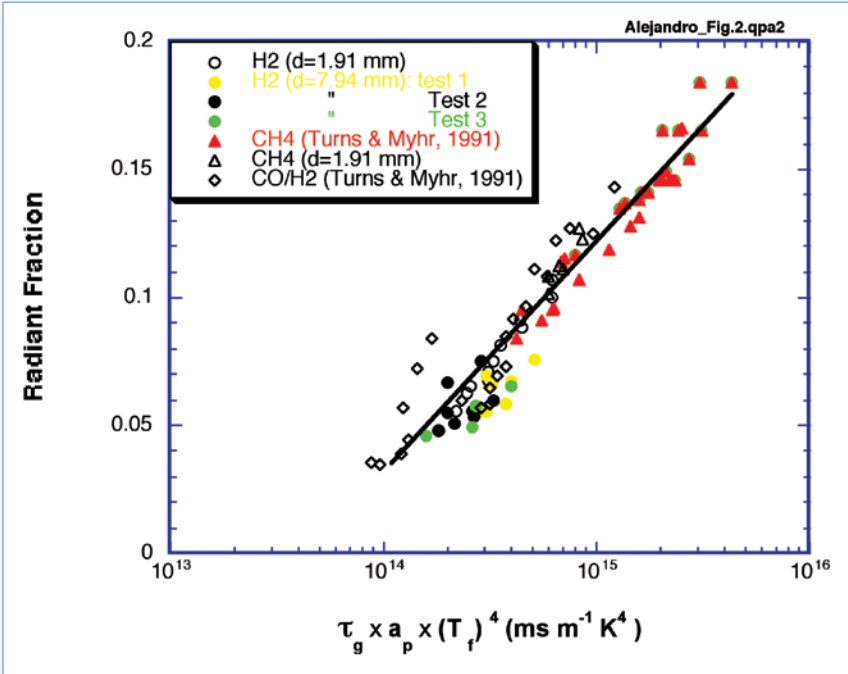


Figure 2. Variation of radiative fraction with the factor τ<sub>g</sub> × a<sub>p</sub> × T<sub>f</sub><sup>4</sup>.

and CO/H<sub>2</sub> that are absent in the hydrogen flames. These bands are strongest for the CO/H<sub>2</sub> flames because of higher CO<sub>2</sub> concentration in the product gases.